JOURNAL OF GUIDANCE, CONTROL, AND DYNAMICS
Vol. 31, No. 4, July–August 2008

Modeling Human Multichannel Perception and Control Using Linear Time-Invariant Models

F. M. Nieuwenhuizen*
Max Planck Institute for Biological Cybernetics, 72012 Tübingen, Germany,
and
Delft University of Technology, 2600 GB Delft, The Netherlands
and
P. M. T. Zaal,† M. Mulder,‡ M. M. van Paassen,§ and J. A. Mulder¶
Delft University of Technology, 2600 GB Delft, The Netherlands

DOI: 10.2514/1.32307

This paper introduces a two-step identification method of human multichannel perception and control. In the first step, frequency response functions are identified using linear time-invariant models. The analytical predictions of bias and variance in the estimated frequency response functions are validated using Monte Carlo simulations of a closed-loop control task and contrasted to a conventional method using Fourier coefficients. For both methods, the analytical predictions are reliable, but the linear time-invariant method has lower bias and variance than Fourier coefficients. It is further shown that the linear time-invariant method is more robust to higher levels of pilot remnant. Finally, both methods were successfully applied to experimental data from closed-loop control tasks with pilots.

Nomenclature

A	=	amplitude
A, B	=	ARX model polynomials
e, E	=	error signal, Fourier transform
f_d, F_d	=	disturbance forcing function, Fourier transform
f_t, F_t	=	target forcing function, Fourier transform
H_c	=	system dynamics
H_{nm}	=	neuromuscular dynamics
H_{pe}	=	error frequency response function
H_{px}	=	state frequency response function
H_v	=	vestibular dynamics
K_m	=	motion perception gain
K_v	=	visual perception gain
k	=	input frequency index
n, N	=	remnant signal, Fourier transform
r	=	signal-to-noise ratio
S	=	power spectral density
u, U	=	control signal, Fourier transform
x, X	=	state signal, Fourier transform
ζ	=	realization of a stochastic process
ζ_{nm}	=	neuromuscular damping
ν, ω	=	frequency
τ_m	=	motion perception time delay
τ_v	=	visual perception time delay
τ_{vl}	=	visual lead time constant
τ_{v1}	=	vestibular lead time constant
τ_{v2}	=	vestibular lag time constant
ω_{nm}	=	neuromuscular frequency

Subscripts

1	=	related to disturbance forcing function
2	=	related to target forcing function

Superscripts

$\hat{}$	=	identified
$\tilde{}$	=	estimated, interpolated

Presented as Paper 6629 at the AIAA Modeling and Simulation Technologies Conference and Exhibit, Keystone, Colorado, 21–24 August 2006; received 19 June 2007; revision received 7 October 2007; accepted for publication 6 November 2007.

*Ph.D. Student, P.O. Box 2169; frank.nieuwenhuizen@tuebingen.mpg.de. Student Member AIAA.

†Ph.D. Student, Control and Simulation Division, Faculty of Aerospace Engineering, P.O. Box 5058; p.m.t.zaal@tudelft.nl. Student Member AIAA.

‡Associate Professor, Control and Simulation Division, Faculty of Aerospace Engineering, P.O. Box 5058; m.mulder@tudelft.nl. Member AIAA.

§Associate Professor, Control and Simulation Division, Faculty of Aerospace Engineering, P.O. Box 5058; m.m.vanpaassen@tudelft.nl. Member AIAA.

¶Professor, Control and Simulation Division, Faculty of Aerospace Engineering, P.O. Box 5058; j.a.mulder@tudelft.nl. Member AIAA.

I. Introduction

COMBINING quasi-linear models and the crossover model theorem [1] has become a well-established paradigm for describing and predicting human control behavior in single-axis compensatory tracking tasks. Methods for the identification of human control behavior in these tasks have been known since the early applications in 1960 [2]. Single-loop methods describe the human controller as a single linear describing function and remnant noise and have been essential tools in many different applications [3–5]. In the early literature, several identification methods have been described in the time and in the frequency domain [6–23]. These single-loop model identification methods and their validation techniques were mathematically formalized for closed-loop estimation [6]. In multiloop situations, model identification becomes more involved. Stapleford et al. [24–26] introduced a suitable technique for multiloop identification in closed-loop control tasks and van Paassen mathematically formalized model validation techniques in 1994 [27]. In other cases where the use of multichannel models was reported, the model identification and validation efforts were not detailed [28–32].

A generalized approach of identification in multiloop compensatory tracking tasks uses Fourier coefficients (FC) [33]. This method has been applied to several problems, such as the identification of pilot control behavior with perspective flight path displays [34], the identification of multimodal control (e.g., in the context of haptic interfaces [27,35]), and the identification of perception and action cycles in the paradigm of active psychophysics

[36–40]. However, the use of Fourier coefficients introduces several constraints in terms of the resolution in the frequency domain, the variance of the identified frequency response functions, and the design of the forcing functions. A new multiloop identification technique, using linear time-invariant (LTI) models, may reduce or eliminate these limitations.

The goal of this paper is to compare the new identification method using LTI models with the conventional method using Fourier coefficients. First, the process of multichannel pilot perception and control and the corresponding multiloop identification problem are discussed, and the previous method using Fourier coefficients is described. Second, the new application of LTI models to the identification problem is elaborated. Third, both identification methods are used in offline simulations with a multimodal, visual/vestibular pilot model. The analytical bias and variance calculations of both methods are validated and the estimated parameters of a multichannel pilot model, the calculated crossover frequencies, and phase margins of multiple simulations are analyzed. Furthermore, the influence of the pilot remnant is investigated. Fourth, the ability of both identification methods to analyze data from a flight simulator experiment is discussed. Finally, conclusions are drawn.

II. Multichannel Perception and Control

The human operator is a nonlinear biological system. However, when trained properly and given constant conditions, the operator can be described by a quasi-linear time-invariant model with a remnant signal that accounts for nonlinear behavior [1]. Many control tasks are inherently multiloop with feedback from visual, somato-sensory, and vestibular cues. Attempts were made to fit multichannel operator models on a single lumped response function [41,42], but this approach led to overparameterization of the model and thus considerable uncertainties in the parameter estimates. To gain better insight into multichannel perception and control more frequency response functions are needed attributing different inputs to the control action of the operator. Thus, a multichannel operator model can be fit more reliably when the problem of overparametrization is reduced.

A multiloop control task is presented in Fig. 1. Here, a human operator is actively controlling the system dynamics H_c, while following a target f_t, and compensating for a disturbance f_d. This allows for the identification of two frequency response functions, H_{pe} and H_{px}, and constitutes a multiloop identification problem. The frequency response functions operate in parallel and represent a response to different perceived inputs. A remnant signal n is added to the output of the operator to account for nonlinear behavior.

A. Multiloop Identification Problem

For the modeling of multichannel perception and control behavior, a two-step method can be applied. In the first step, the frequency response functions, H_{pe} and H_{px} in Fig. 1, are estimated from measured input–output signals. In the second step, the parameters of a multichannel operator model are determined by fitting the model to these estimated frequency response functions.

When considering the first step, the main concern is acquiring appropriate data. As human control behavior is time varying due to factors such as fatigue, it can only be considered constant over a relatively short period of time. As a consequence, the measurement time interval cannot be made arbitrarily long. For estimation, however, long measurement times are required to observe sufficiently low frequencies [33].

Identification of the multiple response functions requires inserting as many deterministic test signals at different locations in the control loop as the number of response functions to be identified. The number of response functions depends on the particular feedback loops that the human operator will close. These feedback loops are determined by the information the operator uses to generate a control signal (e.g., state and velocity information).

Commonly used deterministic test signals for the identification of human control behavior consist of a summation of multiple sine waves with different frequencies [3,33]. When designing these test signals, also known as forcing functions, the requirements for an accurate estimate and the limitations of the human operator and the controlled system have to be taken into account. The requirements for an accurate estimate depend on the method used to identify the frequency response functions, as will be discussed in the next sections. The limitations of the operator mainly pose constraints on the bandwidth of the forcing functions and the amount of power inserted into the closed-loop system. To prevent crossover regression, neither should be too high [1,3]. As the requirements and limitations involved in each can be contradictory, often a tradeoff has to be made.

In the second step of the identification procedure, the multichannel model structure has to be determined [26]. The number and type of perception paths in the multichannel model depend on the performed task and the cues presented to the human operator. As multiple perception paths may be present for one frequency response function, care should be taken such that the model is not overparameterized.

B. Examples

The identification of frequency response functions in multiloop control tasks provides an objective measure for human control behavior in different experimental setups, such as the investigation of the role of multichannel feedback and the investigation and evaluation of augmented flight control systems. Also, the increased use of simulation for training purposes warrants a renewed focus on manual control behavior [43–47]. Multiloop identification methods can be used to assess the effects of, for example, simulator motion on the operator's multichannel perception and control behavior.

An example of a research problem that was analyzed with multiloop identification techniques was an investigation on the use of different modalities to control the roll angle of an airplane [36–38]. This example is illustrated in Fig. 2a. Two forcing functions, a

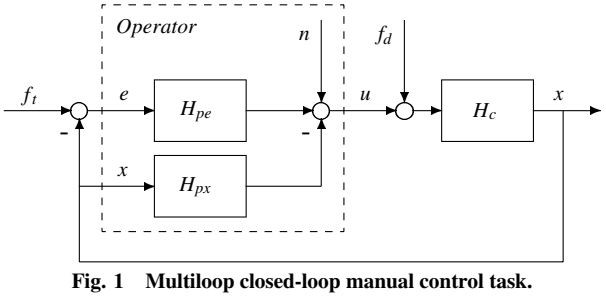

Fig. 1 Multiloop closed-loop manual control task.

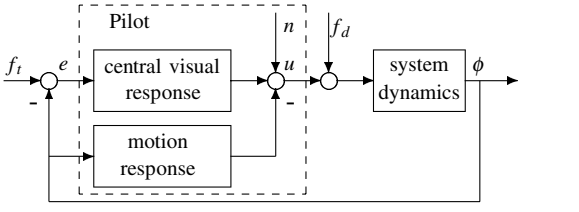

a) Investigation on the use of different modalities in an aircraft roll task

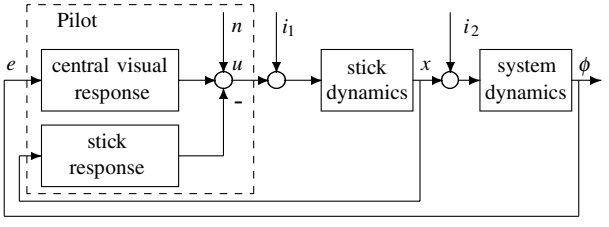

b) Identification of human operator haptic control

Fig. 2 Examples of multiloop control tasks.

disturbance forcing function f_d and target forcing function f_t, are inserted into the loop to allow for the identification of two frequency response functions. The task of the pilot was to minimize the error e perceived via a display with feedback of motion cues. This example, which corresponds to Fig. 1, is used in the remainder of this paper to validate the two identification techniques.

Another example is the identification of human operator haptic control [27,35], which is illustrated in Fig. 2b. In this research, a model was developed to represent the neuromuscular system of a pilot's arm that can be used to design the side-stick in an aircraft more systematically. Also in this research two forcing functions, i_1 and i_2, were used and the task was again to minimize the error e perceived via a display.

III. Conventional Method: Identification Using Fourier Coefficients

The identification method using Fourier coefficients is currently used to estimate frequency response functions in multiloop control tasks and serves as a baseline for benchmarking the identification method using LTI models presented next. The calculations are all performed in the frequency domain and have been described thoroughly before [27,33,34].

A. Identification Procedure

The operator control signal u can be related to the operator inputs in the frequency domain. At an arbitrary input frequency ν_{1j} of forcing function f_d, the following equation holds:

$$U_1 = H_{pe}(\nu_{1j})E_1 - H_{px}(\nu_{1j})X_1 + N_1 \tag{1}$$

Here U_1, E_1, and X_1 denote the Fourier coefficients of the corresponding measured signals at the frequencies of forcing function f_d. To solve Eq. (1) for both operator describing functions, a second equation is obtained by taking the Fourier coefficients of u, e, and x at the frequencies of the target forcing function f_t and interpolating these to the frequencies considered by forcing function f_d. These are denoted by $\tilde{U}_2$, $\tilde{E}_2$, and $\tilde{X}_2$, respectively. The contribution of the remnant noise, N, to the control signal is neglected as, generally, the signal-to-noise ratio is high at the input frequencies [33]. This yields a set of two equations at frequencies ν_{1j} of f_d:

$$\begin{bmatrix} U_1 \\ \tilde{U}_2 \end{bmatrix} = \begin{bmatrix} E_1 & -X_1 \\ \tilde{E}_2 & -\tilde{X}_2 \end{bmatrix} \begin{bmatrix} H_{pe}(\nu_{1j}) \\ H_{px}(\nu_{1j}) \end{bmatrix} \tag{2}$$

From this set of equations, the two operator describing functions can be solved at input frequencies ν_{1j}:

$$\hat{H}_{pe}(\nu_{1j}) = \frac{\tilde{U}_2 X_1 - U_1 \tilde{X}_2}{\tilde{E}_2 X_1 - E_1 \tilde{X}_2}, \qquad \hat{H}_{px}(\nu_{1j}) = \frac{E_1 \tilde{U}_2 - \tilde{E}_2 U_1}{\tilde{E}_2 X_1 - E_1 \tilde{X}_2} \tag{3}$$

The same procedure can be applied for the input frequencies ν_{2j} of forcing function f_t and results in estimates for the two operator describing functions at input frequencies ν_{2j}.

B. Bias and Variance

The contributions of the remnant noise are still present in the estimates of H_{pe} and H_{px} and will influence bias and variance. Analytical expressions for the bias and the variance of the estimates $\hat{H}_{pe}$ and $\hat{H}_{px}$ can be obtained by first determining expressions for all Fourier-transformed signals in the loop (U, E, and X) in terms of signals inserted into the loop (N, F_d, and F_t). These expressions can then be used to evaluate Eq. (3). Definitions for the bias and variance of an estimator are [27]

$$\text{Bias}\,(\hat{H}_{pe}(\nu_{1j})) = -(\hat{H}_{pe})\text{E1} \tag{4}$$

$$\text{Var}\,(|\hat{H}_{pe}(\nu_{1j})|) = |\hat{H}_{pe}|^2(\text{E2} - \text{E1}^2) + \frac{1}{\tilde{r}_2}(1 - 2\text{E1} + \text{E2}) \tag{5}$$

$$\text{Bias}\,(\hat{H}_{px}(\nu_{1j})) = -\left(\hat{H}_{px} + \frac{1}{H_c}\right)\text{E1} \tag{6}$$

$$\text{Var}\,(|\hat{H}_{px}(\nu_{1j})|) = \left|\hat{H}_{px} + \frac{1}{H_c}\right|^2(\text{E2} - \text{E1}^2) + \frac{1}{\tilde{r}_2}(1 - 2\text{E1} + \text{E2}) \tag{7}$$

where E1 and E2, which represent the noise-dependent terms, are given by [6]

$$\text{E}\,1(\nu_{1j};\zeta) = \text{E}\left\{\frac{N_1(\nu_{1j};\zeta)}{F_d(\nu_{1j}) + N_1(\nu_{1j};\zeta)}\right\} = e^{-r_1(\nu_{1j};\zeta)} \tag{8}$$

and

$$\begin{aligned}\text{E2}(\nu_{1j};\zeta) = \text{E}\left\{\left(\frac{N_1(\nu_{1j};\zeta)}{F_d(\nu_{1j}) + N_1(\nu_{1j};\zeta)}\right)^2\right\} &= e^{-r_1+\delta} + e^{-r_1-\delta} \\ - 1 + r_1\int_\delta^{r_1}\frac{e^{p-r_1}}{p}\,\mathrm{d}p + r_1 e^{-r_1}\int_\delta^{\infty}\frac{e^{-p}}{p}\,\mathrm{d}p\end{aligned} \tag{9}$$

These terms can only be calculated when accounting for a small probability ε that the variance is underestimated. The value for ε [$=2e^{-r_1}\sinh(\delta)$] is usually set at 1% [34]. The signal-to-noise ratio of the disturbance forcing function r_1 is defined as the quotient of the power of the deterministic test signal F_d and the power of the stochastic noise signal N_1 at the frequencies ν_{1j} of the test signal f_d. The latter is determined from the averaged power of the control signal at neighboring frequencies of ν_{1j} and ν_{2j}:

$$\begin{aligned}S^2_{N1}(\nu_{1j};\zeta) = S^2_{U_{N1}}(\nu_{1j};\zeta)|1 + H_c(\nu_{1j})(\hat{H}_{pe}(\nu_{1j};\zeta) \\ + \hat{H}_{px}(\nu_{1j};\zeta))|^2\end{aligned} \tag{10}$$

The signal-to-noise ratio of the target forcing function r_2 is defined in a similar way. Similar to the Fourier coefficients, r_2 can be interpolated to the frequencies of the disturbance forcing function, resulting in $\tilde{r}_2$. If the signal-to-noise ratio r_1 at a particular frequency becomes high enough, that is, >5, the expectations E1 and E2 become very small (see Fig. 3). In that case, the bias and variance in the estimated frequency responses at that frequency also become small [34].

The variance of $\angle\hat{H}_{pe}$ in degrees can be approximated with

$$\text{Var}\,(\angle\hat{H}_{pe}(\nu_{1j})) \approx \left(\frac{180}{\pi}\right)^2\frac{\text{Var}(|\hat{H}_{pe}(\nu_{1j})|)}{|\hat{H}_{pe}(\nu_{1j})|^2} \tag{11}$$

A similar expression holds for the variance of $\angle\hat{H}_{px}$.

C. Forcing Function Design

Using the FC method, the operator frequency response functions can only be identified at the input frequencies of the forcing functions, which must meet several constraints. Generally, the input frequencies are multiple integers of a base frequency determined by the sampling time. The input frequencies should cover the frequency range of interest and not be multiple integers of each other. When using more than one forcing function, the frequencies of the different forcing functions should be chosen to be close to each other to avoid interpolation errors. Finally, enough frequency components should be free of energy content to allow for the estimation of variance of the remnant signal needed for the determination of the signal-to-noise ratios.

The number of input frequencies is limited and also the overall power and the bandwidth of the forcing functions should be chosen carefully. An increase in the number of input frequencies, overall power, or bandwidth must result in a decrease in the others, requiring a tradeoff. A randomly selected phase can be introduced at each input frequency to reduce the predictability of the signals and to not provide the human operator with recognizable elements in the

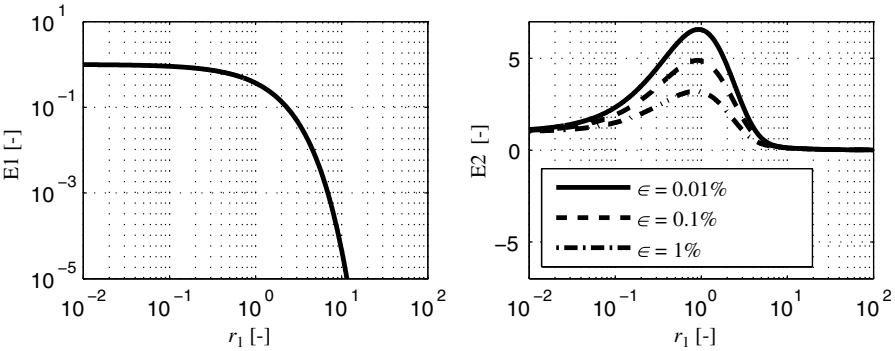

Fig. 3 Expectations E1 and E2.

experiment runs [3]. The forcing functions should be checked for excessive peaks after they are generated.

D. Preprocessing Data from Human-in-the-Loop Experiments

The total experiment time consists of a run-in part and a measurement part. The run-in time is discarded as subjects get accustomed to the control task in this period. To reduce the effect of the remnant and to improve the estimated frequency response functions, time domain data from different runs can be averaged. When the forcing functions for the different experiment runs are the same, averaging the data will result in increased signal-to-noise ratios, a more accurate estimate, and a reduction in the variance of the estimate. There are no stringent demands on the sampling frequency for measuring the data. However, the Nyquist frequency should remain above the highest input frequency of the forcing functions.

IV. Identification Using LTI Models

LTI models, such as the parametric autoregressive exogeneous (ARX) model, are commonly used for system identification of a large variety of dynamical systems [48]. The control behavior of a human operating in a closed-loop control task under constant conditions can also be considered (quasi) linear and time invariant (see Sec. II) and has been identified in single-loop control tasks using LTI models. Therefore, building upon previous research in single loop, it is a logical step to use an LTI model to estimate the operator describing functions, H_{pe} and H_{px}, in a multiloop environment (see Fig. 1).

A. Identification Procedure

The structure of the LTI model used for identification is dependent on the task and the properties of the injected noise [48]. In this paper, the describing functions of an operator in the closed-loop task described in Sec. II are identified with the multi-input–single-output (MISO) ARX model structure. Other LTI model structures, such as ARMAX, Output-Error, or Box–Jenkins, are analogous. The ARX model structure allows for a direct calculation without optimization of the model parameters using a least-squares estimate [48]. The inputs of the LTI model are the measured error signal e and state signal x (see Fig. 4). The remnant of the operator n is described by filtered Gaussian white noise, n_w. The parameters of polynomials A, B_e, and B_x of the ARX model are fit to the control signal of the operator u, using the relationship:

$$u(t) = \frac{B_e(q)}{A(q)}e(t) + \frac{B_x(q)}{A(q)}x(t) + \frac{1}{A(q)}n_w(t) \tag{12}$$

with

$$A(q) = 1 + a_1 q^{-1} + \cdots + a_{n_a} q^{-n_a}$$

and

$$B_{e,x}(q) = b_{1_{e,x}} + b_{2_{e,x}} q^{-1} + \cdots + b_{n_{be,x}} q^{-n_{be,x}+1}$$

Here n_a and $n_{be,x}$ are the orders of the A and B polynomials,

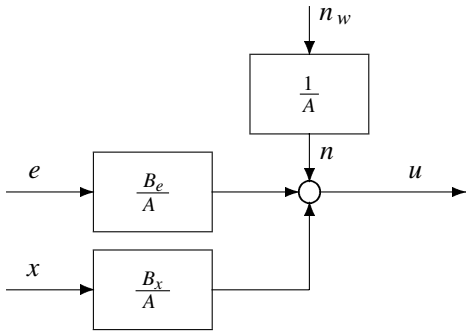

Fig. 4 Multi-input ARX model structure.

respectively. The estimates of the operator describing functions, $\hat{H}_{pe}$ and $\hat{H}_{px}$, are now given by

$$\hat{H}_{pe}(j\omega) = \frac{B_e(j\omega)}{A(j\omega)} \tag{13}$$

$$\hat{H}_{px}(j\omega) = \frac{B_x(j\omega)}{A(j\omega)} \tag{14}$$

where $A(j\omega)$ is the frequency response of the polynomial $A(q)$. The polynomial A gives an estimate of the spectrum of the remnant of the operator (see Fig. 4). These estimates are unbiased (i.e., $\hat{H}_p \to H_p$ for $N \to \infty$, where N is the number of data points) if the remnant is filtered white noise and if the input and output signals are deterministic and bounded sequences [48], as is the case in the closed-loop control task discussed here. Depending on the noise characteristics, other model structures, such as ARMAX, Output-Error, or Box–Jenkins, could result in a more accurate estimate of the describing functions.

The order of the A and B polynomials can be determined by physical insight into the system to be identified. Also, the order of the operator model fit to the describing functions indicates the order of the polynomials of the ARX model. For calculating the orders, a range of techniques is available [48]. An example is to take a range of orders for each polynomial and choose the set of orders that produces the smallest Akaike final prediction error [48].

B. Bias and Variance

The error of the identified operator describing functions with respect to the true operator describing functions is characterized by the bias of the model in closed loop. The bias of the ARX model in closed loop for $\hat{H}_{pe}$ is given by [48]

$$\text{Bias}\,(\hat{H}_{pe}) = \frac{S_{en}(\omega)(\frac{1}{A(\omega)} - \frac{1}{\hat{A}(\omega)})}{S_{ee}(\omega)} \tag{15}$$

where $1/A$ is the true remnant model and $1/\hat{A}$ is the remnant model estimated by the ARX model. S_{ee} denotes the autopower spectral density of the error signal and S_{en} the crosspower spectral density of the error signal and the remnant. A similar expression holds for $\hat{H}_{px}$. From Eq. (15) it can be seen that an erroneous noise model may cause the ARX model to approximate a biased transfer function. Also, any filtering of the signals is equivalent to changing the noise model. Likewise, inappropriate filtering of the measured signals from the experiment may also cause a bias.

The expression for the bias of the estimate contains the true remnant model and the crosspower spectral density of the noise signal with the error signal. The bias cannot be calculated for experiments with pilots in the loop as the true remnant of the pilot is not known in these cases. The bias expressions show that the bias is smaller if the noise model is accurate, the feedback contribution to the input spectrum is small, or the signal-to-noise ratio of the error signal is high. A more accurate noise model can be achieved by carefully choosing the order of the model polynomials, or by applying an appropriate filter to the measured signals, thus minimizing the high-frequency noise contributions. The signal-to-noise ratio of the signal can be increased by inserting more power into the system by increasing the amplitude of the forcing functions.

The variance of the magnitude and the phase of the frequency response of $\hat{H}_{pe}$ and $\hat{H}_{px}$ are given by [48]

$$\mathrm{Var}\,(|\hat{H}_p|) = \frac{\mathrm{Re}(\hat{H}_p)^2 C_1}{|\hat{H}_p|^2} - \frac{2\,\mathrm{Re}(\hat{H}_p)\,\mathrm{Im}(\hat{H}_p) C_3}{|\hat{H}_p|^2} + \frac{\mathrm{Im}(\hat{H}_p)^2 C_2}{|\hat{H}_p|^2} \tag{16}$$

$$\mathrm{Var}(\angle \hat{H}_p) = \left(\frac{180}{\pi}\right)^2 \left(\frac{\mathrm{Im}(\hat{H}_p)^2 C_1}{|\hat{H}_p|^4} - \frac{2\,\mathrm{Re}(\hat{H}_p)\,\mathrm{Im}(\hat{H}_p) C_3}{|\hat{H}_p|^4} + \frac{\mathrm{Re}(\hat{H}_p)^2 C_2}{|\hat{H}_p|^4}\right) \tag{17}$$

with

$$\begin{aligned} C_1 &= \mathrm{Re}\left(\frac{\partial \hat{H}_p}{\partial \theta}\right) P(\theta)\, \mathrm{Re}\left(\frac{\partial \hat{H}_p}{\partial \theta}\right)^* \\ C_2 &= \mathrm{Im}\left(\frac{\partial \hat{H}_p}{\partial \theta}\right) P(\theta)\, \mathrm{Im}\left(\frac{\partial \hat{H}_p}{\partial \theta}\right)^* \\ C_3 &= \mathrm{Re}\left(\frac{\partial \hat{H}_p}{\partial \theta}\right) P(\theta)\, \mathrm{Im}\left(\frac{\partial \hat{H}_p}{\partial \theta}\right)^* \end{aligned} \tag{18}$$

Here C_1, C_2, and C_3 are the entries of the covariance matrix for the real and imaginary parts of the Fourier coefficients of $\hat{H}_{pe}$ or $\hat{H}_{px}$. In Eq. (18), $*$ denotes the complex conjugate transpose, θ is the parameter vector of the ARX model consisting of the coefficients in Eq. (12), $P(\theta)$ is the parameter covariance matrix of the model, and $\partial \hat{H}_p / \partial \theta$ is the sensitivity of $\hat{H}_p$ with respect to the parameter set.

C. Forcing Function Design

An advantage of the identification method using LTI models is that no stringent requirements are imposed on the input frequencies, as was the case with the FC method discussed in Sec. III. The forcing functions are not required to be multisine signals, but only need to be measurable. However, some other important requirements for the forcing functions still remain. To properly identify the operator describing functions in a closed-loop control task, the inputs to the operator, e and x, should be "informative" [48]. This means that the inputs and thus the forcing functions should only give rise to one possible estimate of the operator describing functions. Furthermore, the input power of the forcing functions should be as high as possible, maximizing signal-to-noise ratios to minimize the variance in the estimate, and the bandwidth of the forcing functions should be such that the describing functions can be identified in the frequency range of interest.

D. Preprocessing Data from Human-in-the-Loop Experiments

The signals used for identification often consist of a useful part, up until a certain frequency, and a disturbance part, the high-frequency noise contributions. For identification of the operator describing functions, the sampling frequency should not be too high, as the high-frequency noise contributions are not of interest and should not be captured by the LTI model. On the other hand, it is important that the sampling frequency, and thus the Nyquist frequency, is high enough to capture all the useful information. The choice of sampling frequency for measuring the data is thus very important for the noise reduction in the estimate.

When considering experiments, the sampling frequency of the measured data is often fixed by the experimental software or equipment and can be much higher than needed. In this case, the data should be resampled to eliminate the noise contributions. Then, however, an antialiasing filter must be applied before the data are resampled in order to not let the folding effect distort the interesting part of the spectrum below the Nyquist frequency [48]. The cutoff frequency of the filter should be higher than or equal to the Nyquist frequency of the resampled signal.

Bursts and outliers in the measured data that are the result of the nonlinear behavior of the operator are also unwanted effects. As we are estimating an LTI model to describe the operator control behavior, the nonlinear effects should be eliminated before the identification procedure. This can be done by averaging the measured data from different experimental runs of the same condition, similar to the FC method discussed in Sec. III.

V. Offline Simulations

In this section, the identification methods are validated with the use of Monte Carlo simulations of the multiloop structure presented in Fig. 1.

A. Method

The conventional FC method and the new LTI method are applied to the output of 10,000 simulations of a pilot model controlling the roll angle of an airplane (see Fig. 2a). The system dynamics are a double integrator, $H_c = 4/s^2$, as used in similar studies [36,37]. Figure 1 shows the multichannel structure where the pilot perceives visual and physical motion cues originating from the controlled system dynamics H_c. A target signal f_t and a disturbance signal f_d are inserted into the loop to allow for the identification of the error frequency response function H_{pe} and the state frequency response function H_{px} of the pilot. Using these two forcing functions, the task of the pilot is a target-following task in which the aircraft is in turbulent conditions. The pilot perceives the error e and the error rate $\dot{e}$ via a visual display, and the aircraft roll accelerations, which result from a change in the roll state x, are felt through the vestibular system.

The multichannel pilot model used for simulations is given in Fig. 5. It is based on the models proposed by van der Vaart [41] and Hosman [42] and consists of a pilot visual perception path, a vestibular motion perception path, and the neuromuscular dynamics H_{nm}. The error response function H_{pe} in Fig. 1 is a combination of the visual perception path, that processes error and error rate, and the neuromuscular dynamics. Similarly, the state response function H_{px} is a combination of the vestibular motion perception path and the neuromuscular dynamics. The model is built up from the sensor dynamics in the motion perception path (i.e., the vestibular dynamics H_v), the equalization, which is a combination of gains and time constants, and the pilot limitations, which consist of the time delays of the perception paths and the neuromuscular dynamics. The pilot adapts his equalization for the controlled dynamics in such a way that the total open-loop response is an integrator near the crossover frequency [3].

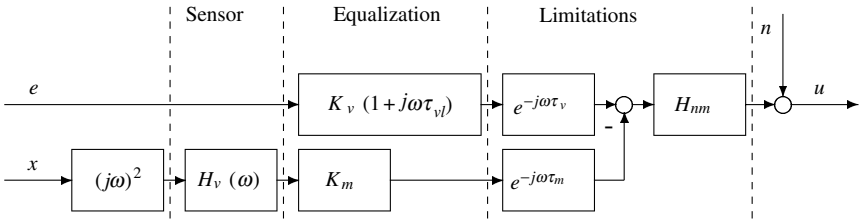

Fig. 5 Multichannel pilot model used for simulations.

The vestibular dynamics are modeled using a model of the semicircular canals sensing rotational accelerations [42,49]:

$$H_v = \frac{1 + j\omega\tau_{v1}}{1 + j\omega\tau_{v2}} \tag{19}$$

The neuromuscular dynamics of the pilot are modeled by [34]

$$H_{nm} = \frac{\omega_{nm}^2}{\omega_{nm}^2 + 2\zeta_{nm}\omega_{nm}j\omega + (j\omega)^2} \tag{20}$$

The remnant n consists of Gaussian white noise, filtered with a second-order low-pass filter [50,51]:

$$n = \frac{0.2(3.0s + 1)}{(1.5s + 1)(0.4s + 1)} n_w \tag{21}$$

With this filter, the total power of the remnant signal is scaled to 10% of the power of the pilot control signal u. This filter intentionally does not resemble the remnant filter shape assumed by the ARX model.

The values for the parameters of the multichannel pilot model are taken from previous experiments [41] and are given in Table 1.

In previous sections, the requirements for the two forcing functions were discussed for each identification method. Each forcing function is based on a sum of 12 sinusoids, with the frequencies ω_i and amplitudes A_i given in Table 2. Subscripts 1 and 2 refer to the disturbance and target forcing function, respectively. The frequencies of the forcing functions are all multiple integers, given by k_1 and k_2, of a base frequency that is the inverse of the measurement time of $81.92s$. No random phase is introduced at the input frequencies. The distribution of amplitudes A_i is determined with the following filter:

$$H_f = \frac{(s + 10)^2}{(s + 1.25)^2} \tag{22}$$

When considering disturbance tasks, the shaping filter is affected by an attenuation of the system dynamics, H_c. Therefore the amplitude of the disturbance forcing function was prefiltered with the inverse system dynamics.

Each simulation used the same parameters for the pilot model and the forcing functions, but a randomly generated pilot remnant. This simulates a well-trained pilot in different experimental runs under the same conditions. Typical time domain histories of the signals in the loop (e, u, x, and n) for one simulation are given in Fig. 6. In particular, one can see the amount of the remnant with respect to the control signal u. Finally, the figure shows the forcing functions, f_d and f_t, where the disturbance forcing function has been prefiltered with the inverse system dynamics, resulting in much higher frequency content.

The power spectral densities of all signals are given in Fig. 7. The contributions of the forcing functions to each signal in the loop are distinguishable. From the power spectral density of the forcing functions one can see the shape of the second-order filter used to create the amplitudes of the forcing functions and the recovering of the amplitudes from the second-order filter shape at higher frequencies.

Table 1 Pilot model parameters

Parameter	Value
τ_{v1} vestibular lead time constant	0.10 s
τ_{v2} vestibular lag time constant	6.00 s
K_v visual perception gain	0.17 –
τ_{vl} visual lead time constant	2.93 s
K_m motion perception gain	1.59 –
τ_v visual perception time delay	0.32 s
τ_m motion perception time delay	0.29 s
ω_{nm} neuromuscular frequency	12.0 rad/s
ζ_{nm} neuromuscular damping	0.30 –

Table 2 Forcing functions definition, with k_i the number of periods that fit within the measurement time, ω_i the frequency, and A_i the amplitude of the sinusoid

Disturbance			Target		
k_1, –	ω_1, rad/s	A_1, rad	k_2, –	ω_2, rad/s	A_2, rad
5	0.3835	0.0020	6	0.4602	0.0568
8	0.6136	0.0046	9	0.6903	0.0495
11	0.8437	0.0074	13	0.9971	0.0397
17	1.3039	0.0125	19	1.4573	0.0278
28	2.1476	0.0184	29	2.2243	0.0162
46	3.5282	0.0235	47	3.6049	0.0078
59	4.5252	0.0264	61	4.6786	0.0052
82	6.2893	0.0316	83	6.3660	0.0034
106	8.1301	0.0382	107	8.2068	0.0024
137	10.507	0.0489	139	10.661	0.0019
178	13.652	0.0669	179	13.729	0.0015
211	16.183	0.0848	213	16.336	0.0014

B. Results

This section gives the results from the offline simulations. Note that the Fourier coefficient method is a spectral nonparametric method, while the method using LTI models is parametric. Therefore, the latter method should perform better considering that more knowledge is incorporated into the estimators (e.g., about the remnant).

1. *Identification*

A bode plot of the identified pilot frequency response functions, $\hat{H}_{pe}$ and $\hat{H}_{px}$, of one simulation using both methods is given in Fig. 8. From this figure it can be seen that the Fourier coefficient method only gives an estimate at the 24 input frequencies of the forcing functions, whereas the method using ARX models gives a continuous estimate. It can be seen that for this condition the Fourier coefficient method produces less accurate results. On the contrary, the estimates from the ARX model follow the analytical frequency response functions of the pilot model better. The standard deviations of the estimates from the Fourier coefficient method in Fig. 8 are calculated using Eqs. (5), (7), and (11) and are represented by the vertical bars. For lower frequencies, the standard deviations are higher as the signal-to-noise ratios are lower (see Fig. 7). The standard deviations of the estimates from the ARX model are calculated using Eqs. (16) and (17) and are given by the continuous dashed lines. The standard deviation of the ARX estimate is larger for frequencies below or above the input frequencies of the forcing functions.

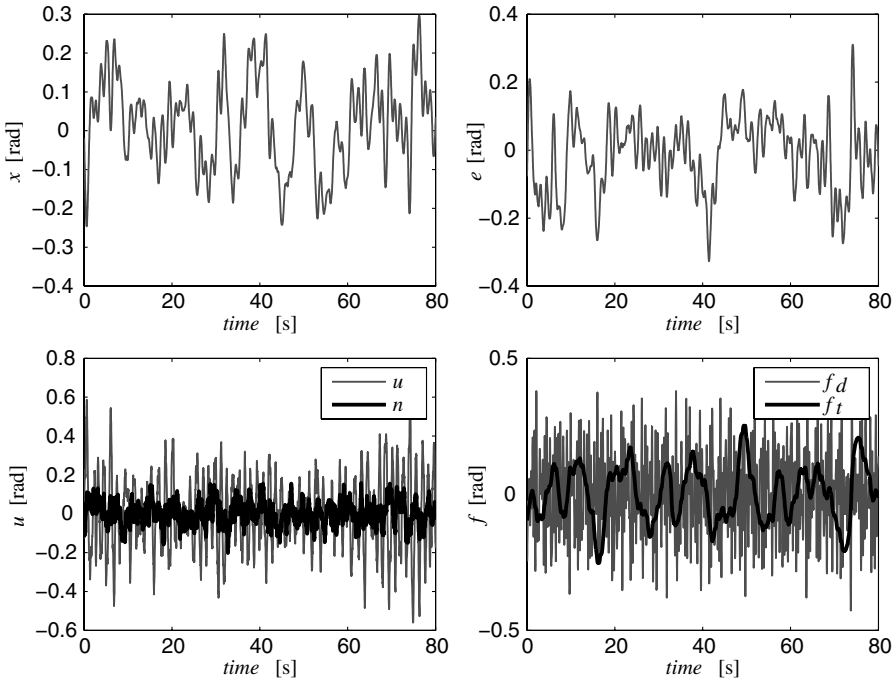

Fig. 6 Time domain representations of state signal x, error signal e, control signal u, and forcing functions f_d and f_t.

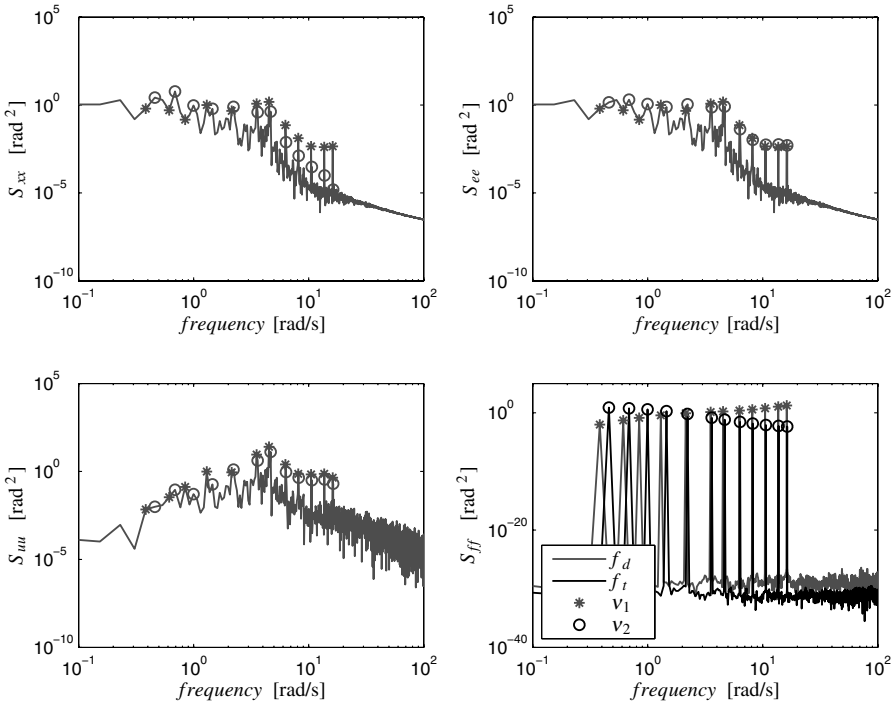

Fig. 7 Power spectral densities of state signal x, error signal e, control signal u, and forcing functions f_d and f_t.

2. Variance

In Fig. 9 the standard deviations of both identification methods are compared. Also, the analytically calculated standard deviations from Eqs. (5), (7), (16), and (17) are averaged and compared to the sample standard deviations estimated from 10,000 simulations in order to validate the correctness of the equations. It can be seen that the standard deviations from the ARX model estimates are much lower than the ones from the Fourier coefficient estimates. It can also be seen that the mean analytically calculated standard deviations and the standard deviations of 10,000 simulations coincide very well for the ARX model method. For the Fourier coefficient method, the assumption of leaving out the remnant term of the equations of the standard deviations results in a slightly worse approximation of the real standard deviations of 10,000 simulations. Also, an error results by allowing a probability of underestimating the variance ε in Eq. (9).

3. Bias

The bias is calculated for the estimates of both identification methods using the equations from Secs. III and IV. Because of the high signal-to-noise ratios at the input frequencies of the forcing functions, it is close to zero. However, the mean bias of 10,000 simulations is much higher than the analytically calculated bias. To

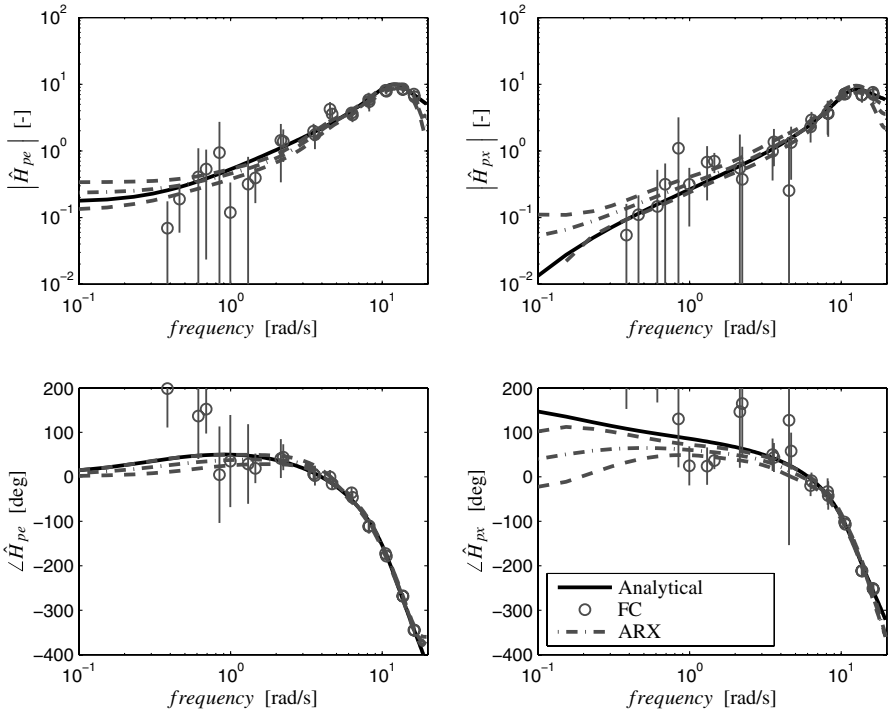

Fig. 8 Bode plot of the identified frequency responses, estimated variances, and the analytical pilot model.

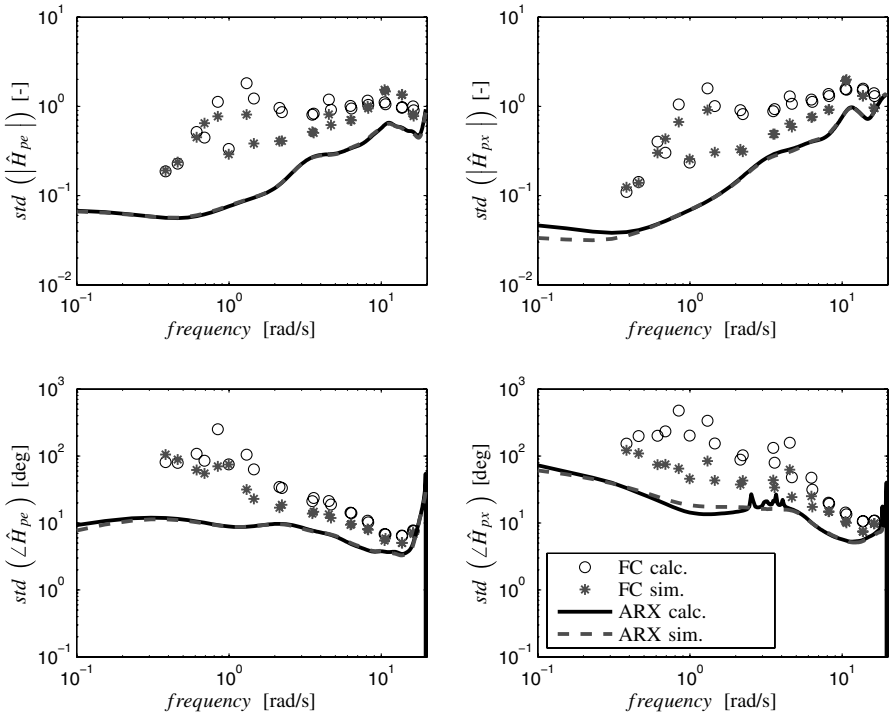

Fig. 9 Standard deviation of the identifications (calculated using the analytical equations for the variance and the variance estimated from 10,000 simulations).

investigate if this bias is significant, it is compared with the 99% confidence interval of the estimates for the Fourier coefficient and the ARX model identification method in Figs. 10a and 10b, respectively. From these figures, it can be seen that the bias of the simulations lies mostly within the 99% confidence interval of the estimates, meaning that it is not significant. For the ARX model identification method, the bias of the simulations is larger than the confidence interval for $|\hat{H}_{pe}|$ and $\angle\hat{H}_{px}$ at very high frequencies. This can be expected as these frequencies lie above the highest input frequency of the forcing functions. Apparently, the ARX model cannot provide a reliable estimate beyond this frequency.

4. *Parameter Estimation*

The identified frequency response functions serve as the input for the parameter estimation procedure in which the parameters of the multichannel pilot model, given in Sec. V.A, are estimated. The vestibular dynamics of the multichannel pilot model, Eq. (19), are assumed constant. The frequency responses of the parameter model resulting from both identification methods, $\tilde{H}_{pe}$ and $\tilde{H}_{px}$, are given in Fig. 11. The parameter estimations from both identification methods give good results. The means and the 95% confidence intervals of the estimated parameters (Fig. 12) show that using the identification with ARX models results in less variability in the estimated parameters.

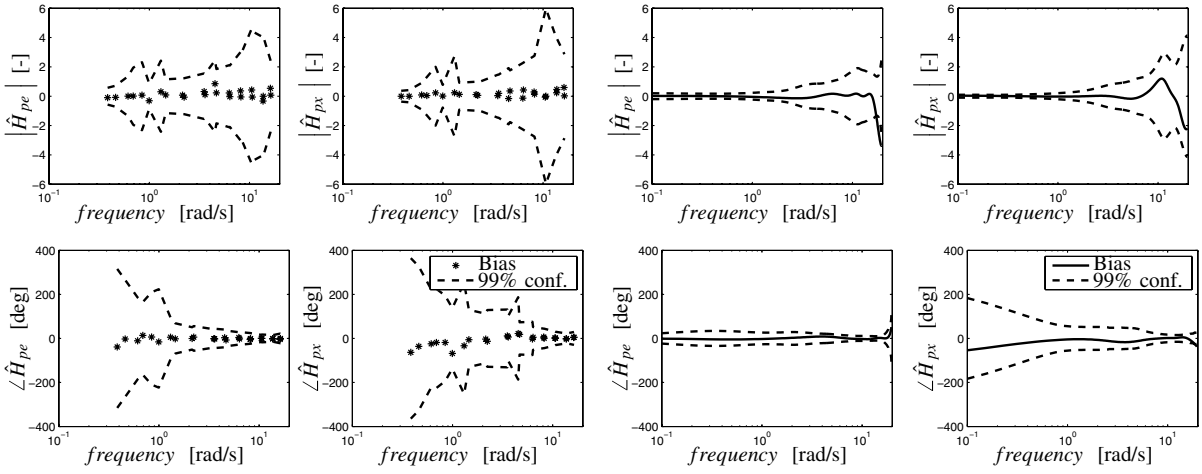

a) FC identification **b) ARX identification**

Fig. 10 Mean bias of the identified frequency responses (10,000 simulations).

This can be attributed to the lower variance of the ARX model estimate and the fact that it is continuous. Also, the bias in the parameters is generally lower than with the method using Fourier coefficients. The mean values of the absolute error of the parameters of 10,000 simulations are given in Table 3. This measure shows how well the parameters are estimated. One can see that the error of the parameters estimated using the ARX model identification as input is always lower.

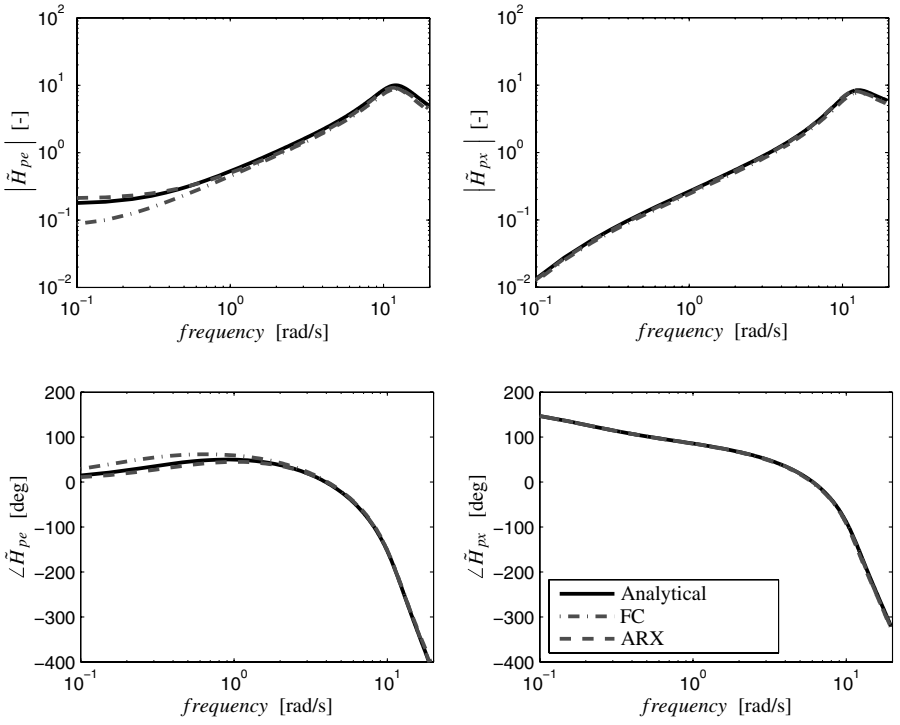

Fig. 11 Bode plot of the parameter estimations.

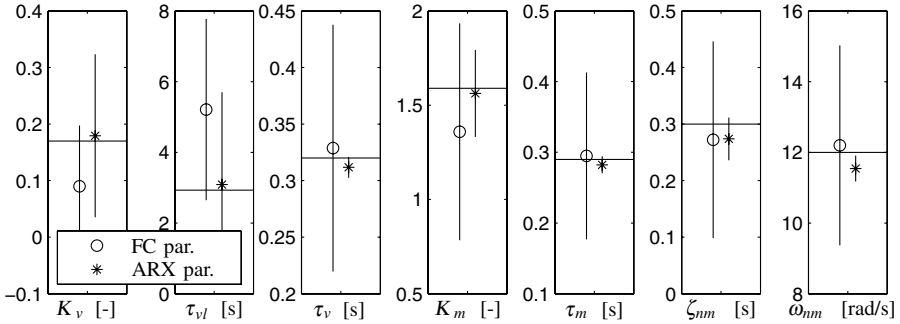

Fig. 12 Parameter means and 95% confidence intervals (10,000 simulations).

Table 3 Absolute error of the estimated parameters

	FC	ARX
K_v, –	8.98×10^{-2}	5.84×10^{-2}
τ_{vl}, s	2.44	1.05
τ_v, s	1.38×10^{-2}	8.44×10^{-3}
K_m, –	2.71×10^{-1}	9.64×10^{-2}
τ_m, s	1.38×10^{-2}	8.31×10^{-3}
ζ_{nm}, –	5.87×10^{-2}	2.76×10^{-2}
ω_{nm}, rad/s	6.56×10^{-1}	4.62×10^{-1}

5. Statistics, Crossover Frequency, and Phase Margin

The statistics, elaborated in the Appendix, the crossover frequencies f_c and phase margins p_m, are summarized in Fig. 13 for the identifications and parameter estimations. The figure shows the means and the 95% confidence intervals of the root mean squared error (RMSE), weighted mean squared error (WMSE), and the summed mean variance (SMV) for 10,000 simulations. The statistics for the identification and parameter estimate of the method using ARX models always have the lowest value compared to the method using Fourier coefficients, meaning that they are more accurate and have a lower variance. Also, the crossover frequency and phase margin are estimated more accurately with the identification and parameter estimate using ARX models. An explanation for this is that the ARX model estimate is continuous, and thus there are less interpolation errors. For the phase margins of the frequency responses estimated with the Fourier coefficient method, large errors are present due to interpolation errors.

The results from 10,000 simulations presented in Figs. 12 and 13 were analyzed using an analysis of variance (ANOVA). This analysis showed that the better performance of the ARX model identification and the resulting parameter estimation was indeed highly significant for all estimated parameters and calculated statistical measures ($p < 0.05$).

6. Remnant

For the previous results, one specific remnant level was used and the ARX model identification method performed better. Coherence functions, defined in the Appendix, can be used to investigate the influence of the remnant level. A coherence function is a measure of the linearity in response to the external inputs. When the coherence function is close to 1, the power of any noise is relatively small and the output is almost linearly related to the input. Figures 14a and 14b give the ordinary coherences of the disturbance forcing function and the target forcing function to the control signal, γ_{fd} and γ_{ft}, respectively. In these figures, the coherence is shown as a function of the ratio of the remnant power and the control signal power. A value of 0.1 means that 10% of the power of the control signal is contributed by the remnant. The figures show that the coherence is close to 1 for all frequencies at the lowest remnant power ratio. As the ratio increases, the coherence decreases and more nonlinearities are captured in the estimates. This trend is also present in Fig. 15, which shows the statistics from Fig. 13 as a function of the remnant power ratio. It can be seen that for both $\hat{H}_{pe}$ and $\hat{H}_{px}$ the ARX estimate gives the best results (i.e., the highest accuracy and the lowest variance). The accuracy of the Fourier coefficient method decreases more rapidly and the variance increases more rapidly as the remnant power ratio increases. This shows that the ARX model estimate is more reliable with increasing pilot remnant.

VI. Flight Simulator Experiment

In this section, both identification methods are used for the evaluation of experimental data derived from a flight simulator evaluation.

A. Method

In a previous experiment [37], the use of central visual and vestibular motion cues in a target and a disturbance control task was investigated by looking at pilot control behavior. The experiment was conducted in the SIMONA Research Simulator (SRS), a 6-degrees-of-freedom full-motion flight simulator. Four subjects performed a closed-loop roll control task compensating for two forcing functions using a electrohydraulic control column. A double integrator with a gain of four was used for the system dynamics. The error between the target forcing function and the roll angle was shown on a compensatory central visual display (see Fig. 2a). No outside visual was used. In the experiment exclusive stimulation of the semicircular canals was attempted by adjusting the simulator motion in such a way that the center of rotation was at the position of the pilot's head. No motion filter was used. Distinct target following and disturbance rejection tasks were created by scaling the disturbance and target forcing function amplitudes by a factor of half, respectively. Also the effect of vestibular cues was investigated by using either full motion of the simulator or motion reduced by a factor of half. This resulted in four experimental conditions.

Both identification methods are used to identify pilot control behavior for the two motion conditions of the disturbance task. The target task is not considered here. During the experiment, each pilot performed 10 trials per condition and the recorded signals were

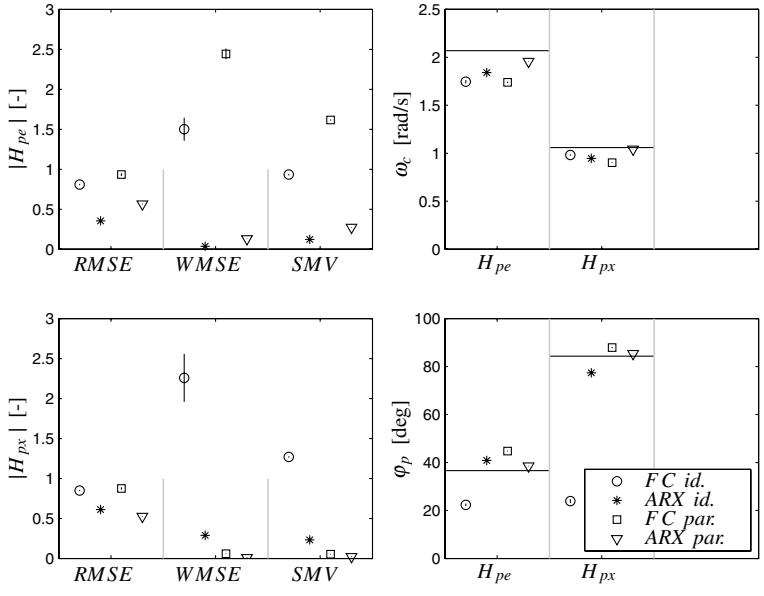

Fig. 13 Means and 95% confidence intervals of the statistics for identifications and parameter estimates (10,000 simulations).

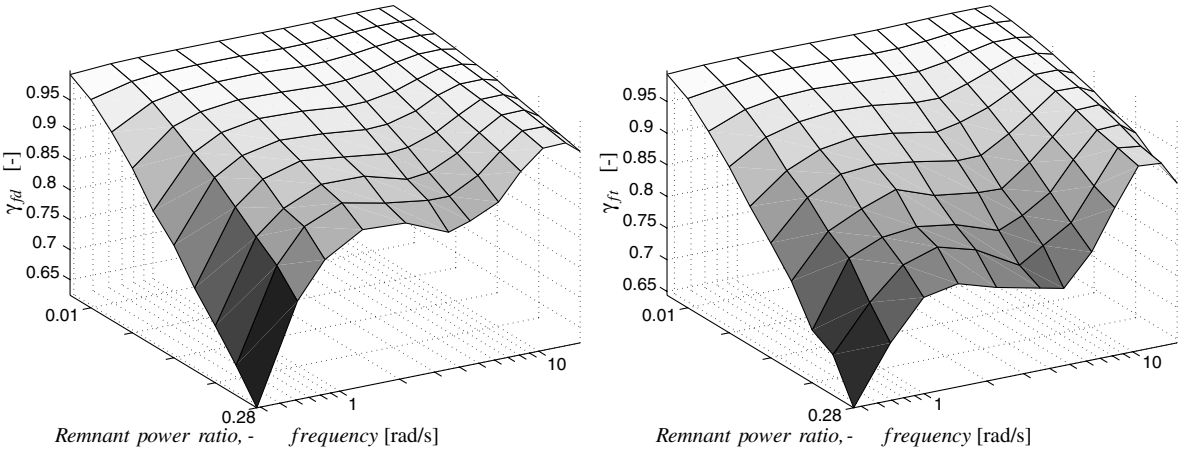

a) Disturbance forcing function **b) Target forcing function**

Fig. 14 Coherence with respect to the control signal as a function of the remnant power ratio.

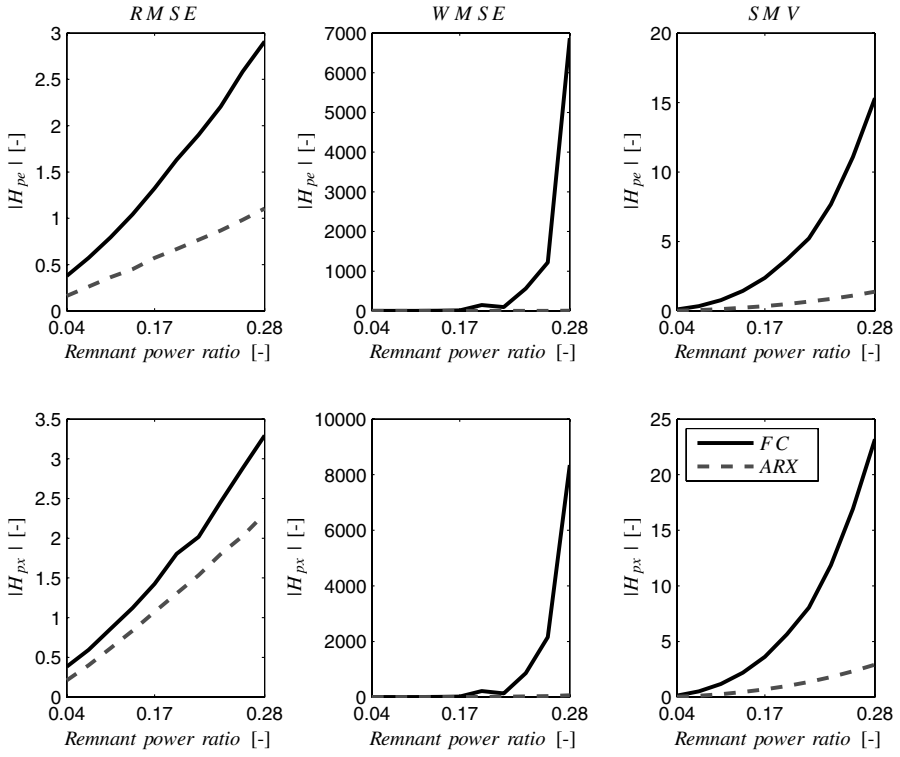

Fig. 15 Statistics as a function of the remnant power ratio.

averaged before identification. In a second step, the parameters of a multichannel pilot model were estimated by fitting the model to the identified frequency response functions.

B. Results

The identified frequency responses for the disturbance task with reduced motion for one subject are given in Fig. 16. The identified points of the frequency response functions of both methods show very good resemblance, partly due to the averaging of experiment runs. However, the variance of the method using Fourier coefficients still is high at several frequencies, as in the offline simulations. The frequency response functions of the method using ARX models clearly provide better insight into the parameters of the underlying pilot model as they are continuous in the frequency domain and have low variance.

The variance accounted for (VAF) (see the Appendix) of the ARX model estimated on the averaged data from 10 experimental runs is very high, at around 95%, for every condition. This was expected as the remnant is eliminated by averaging and, as a result, the ARX models give a good identification despite the simple noise model. If an ARX model is estimated with the data of one run, the VAFs are approximately between 85 and 90%. Box–Jenkins models, which have the most freedom in modeling the remnant, result in VAFs that are only 1 to 2% higher.

In Fig. 17, the frequency response functions of the estimated pilot model are given for the two motion conditions with a disturbance task. The reduction of motion affects the visual perception frequency response H_{pe} and the motion perception frequency response H_{px}. The parameters for the full-motion case and the reduced motion case are given in Table 4. With reduced motion, the visual perception gain is higher. The neuromuscular damping and the neuromuscular frequency are smaller for the reduced motion condition. The parameters of the multichannel pilot model fit on the Fourier coefficient estimates and on the ARX estimates show similar behavior.

As only one parameter estimate is available for every condition due to averaging, the variance of the parameters cannot be calculated. The Cramer–Rao lower bound (CRLB) is a lower bound for the

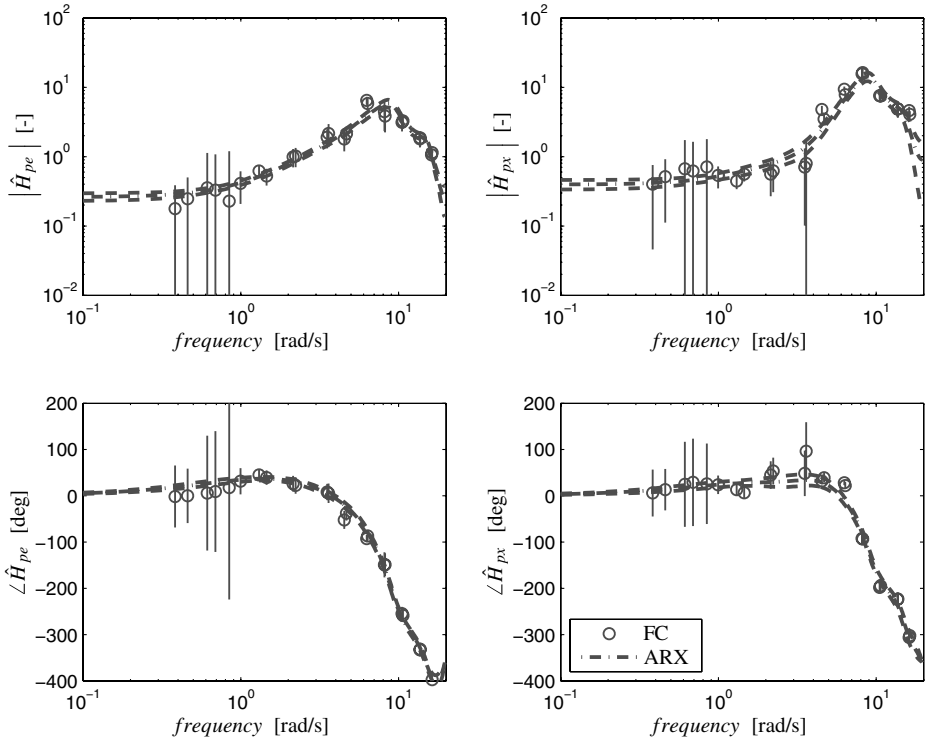

Fig. 16 Bode plot of the identified frequency responses.

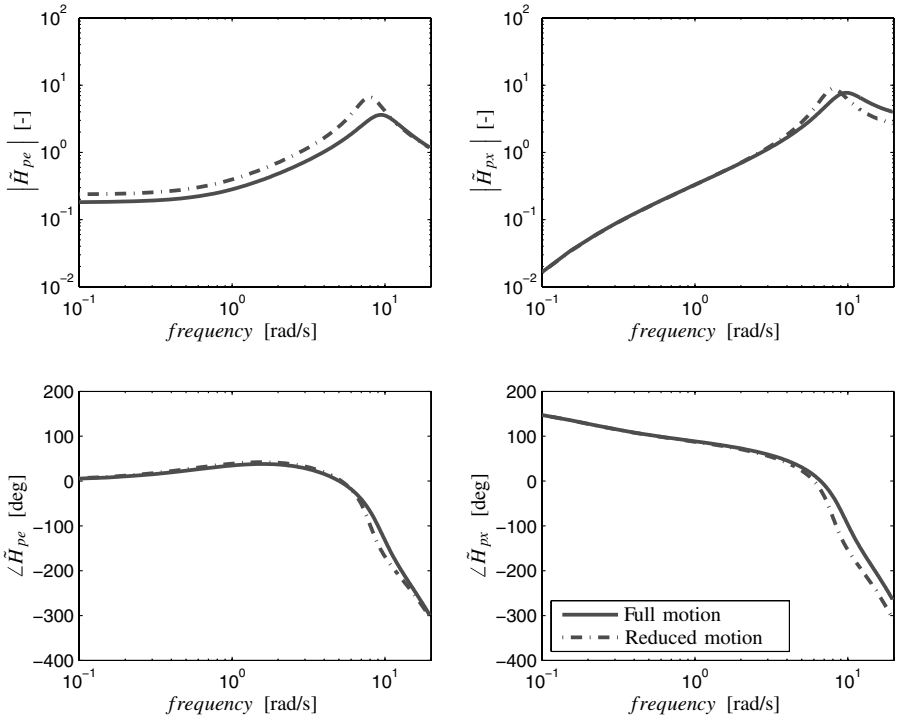

Fig. 17 Bode plot of the parameter estimations.

variance of the estimated parameters and can be calculated analytically for every parameter estimate (see the Appendix). The CRLB for the estimated parameters is also given in Table 4. The CRLB for the parameters estimated using the ARX estimate is much lower than the CRLB for the parameters estimated using the Fourier coefficients. This is consistent with the results found in the previous section.

VII. Discussion of Results

The methods examined in this paper allow for the identification of multichannel human perception and control behavior in active closed-loop control tasks. The methods are inherently different: the conventional one is a spectral method using Fourier coefficients and the novel one a parametric method using LTI models, in this paper ARX models.

1) Statistical measures show that the LTI model frequency response estimate is more accurate and has a lower variance. Also, the standard deviation is much lower than the standard deviation of the Fourier coefficient method. This is the case as the identification method using LTI models specifically accounts for the remnant in the estimations of the pilot describing functions.

2) The mean analytically calculated variance of both methods shows good resemblance with the variance found in multiple

Table 4 Comparison of the estimated parameters for the two motion conditions

	Reduced motion				Full motion			
	FC	ARX	FC CRLB	ARX CRLB	FC	ARX	FC CRLB	ARX CRLB
K_v, –	0.27	0.24	5.37×10^{-2}	1.23×10^{-3}	0.15	0.18	1.89×10^{-2}	1.16×10^{-3}
τ_{vl}, s	0.85	1.32	6.14×10^{-1}	5.49×10^{-2}	1.12	1.18	1.49	7.89×10^{-2}
τ_v, s	0.20	0.20	3.86×10^{-4}	9.10×10^{-5}	0.22	0.20	1.46×10^{-3}	1.88×10^{-4}
K_m, –	2.22	1.96	2.15	7.26×10^{-2}	2.13	1.98	7.71×10^{-1}	1.84×10^{-2}
τ_m, s	0.25	0.26	3.05×10^{-1}	4.33×10^{-2}	0.24	0.23	1.43×10^{-1}	1.18×10^{-2}
ζ_{nm}, –	0.12	0.19	4.28×10^{-3}	1.62×10^{-3}	0.33	0.28	8.66×10^{-2}	4.98×10^{-3}
ω_{nm}, rad/s	8.14	7.93	2.33×10^{-1}	7.20×10^{-2}	10.2	9.42	3.63	2.81×10^{-1}

simulations. Therefore, the analytical calculations can be trusted to provide accurate results.

3) For both methods, the bias of the estimates found in multiple simulations is always within the 99% confidence interval of the estimates for the range of input frequencies of the forcing functions. This is due to high enough signal-to-noise ratios. Therefore, the bias is not significant in this range.

4) The LTI model identification method gives the best results when estimating the parameters of a multichannel pilot model. Also, the variance of the parameters is much lower for the LTI model identification. This is because the LTI model estimate, which is the input for the parameter estimation procedure, already has a lower variance and is continuous in the frequency domain.

5) Key variables such as the crossover frequency and phase margin can be estimated more accurately with the LTI model method. The Fourier coefficient method can introduce large interpolation errors when estimating these quantities.

6) With increasing the pilot remnant, the method using LTI models continues to perform better than the method using Fourier coefficients and is therefore more robust.

7) The identification methods were successfully applied to experimental data of closed-loop control tasks with human operators in the loop. The identified frequency response functions show similar characteristics to the results of the Monte Carlo simulations and the parametric estimations show clear changes with different experimental conditions.

8) The method using LTI models is easier to use when doing research on pilot multimodal perception and control, as the forcing functions are easier to construct, require less tuning, and the method is more intuitive.

Future research focuses on the use of different LTI models, such as ARMAX, Output-Error, or Box–Jenkins, for use with identification. These model structures have the potential to deliver better estimates due to the use of different polynomials for the description of the remnant. Also, the effect of different remnant characteristics on the various LTI models needs to be investigated further.

VIII. Conclusions

A method for the identification of human control behavior using LTI models was compared with a spectral method using Fourier coefficients. For both methods, the analytical calculations of bias and variance were validated successfully with the use of 10,000 closed-loop simulations. The novel method using LTI models performed significantly better than the spectral method in terms of estimating the pilot model parameters and the calculated statistical measures. The main reasons for this are that the method using LTI models assumes a model structure and incorporates the pilot remnant. Consequently, the identified frequency response functions are better and the variance of the estimates is smaller. Further, the parameter estimates of the pilot model are more veridical and have lower variance. The proposed method is also more robust to higher levels of pilot remnant than the method using Fourier coefficients. Although both methods were successfully applied to experimental data of closed-loop, multichannel control tasks, the method using LTI models more clearly revealed the effects of the experimental conditions due to the lower variance found in the parameter estimates.

Appendix: Validation Measures

Statistics

The statistics used for comparison of the two identification methods include the root mean squared error, the weighted mean squared error, and the summed mean variance [see Eq. (A1)]. The RMSE quantifies the error between the estimate and the true pilot response function. The WMSE is comparable to the RMSE, but weighted with the variance of the estimates. This gives a measure of the quality of fit in combination with the variance. Finally the SMV is a measure of the amount of variance in the estimates. For both identification methods the statistics are determined using only the data on the input frequencies. The crossover frequencies and phase margins are also used as a measure of the quality of fit. These are determined from the separate open-loop dynamics of the error response function and the state response function of the identifications and parameter estimations:

$$\text{RMSE} = \sqrt{\frac{1}{N}\sum_{i=1}^{N} e_i^2}, \qquad \text{WMSE} = \frac{1}{N}\sum_{i=1}^{N}\frac{e_i^2}{\sigma_i^2}$$
$$\text{SMV} = \frac{1}{N}\sum_{i=1}^{N}\sigma_i^2 \tag{A1}$$

Coherence Functions

Coherence functions are used as a measure of the statistical validity of the estimated transfer functions and reveal the presence of nonlinearities, extraneous noise, or the existence of uncorrelated inputs. The coherence functions [given in Eq. (A2)] show the degree to which the output of a system is linearly related to the external inputs and have a value between zero and unity. The power spectral densities $S_{f_d u}$, $S_{f_d f_d}$, and S_{uu} are estimated by calculating the mean of the power spectral densities of different runs:

$$\gamma^2_{f_d u} = \frac{|S_{f_d u}|^2}{S_{f_d f_d} S_{uu}}, \qquad \gamma^2_{f_t u} = \frac{|S_{f_t u}|^2}{S_{f_t f_t} S_{uu}} \tag{A2}$$

Variance Accounted for

The VAF is a metric for validating an estimated model and shows how well the model can predict the measured output signal. The metric has a value between 0 and 100%, with 100% indicating that the signal can be perfectly simulated by the LTI model. The metric can be calculated for signal u in the following manner:

$$\text{VAF} = \left(1 - \frac{\sum |u - u_{\text{sim}}|^2}{\sum u^2}\right) \times 100\% \tag{A3}$$

Cramer–Rao Lower Bound

The CRLB gives a lower bound for the covariance matrix of an estimate $\hat{\theta}$ of the parameter vector and is defined as the inverse of the Fisher information matrix, given as

$$M_{\theta\theta} = E\left\{\frac{\partial^2 J(\theta)}{\partial\theta\partial\theta}\right\}$$
$$= \frac{2}{N_f}\,\mathrm{Re}\left\{\sum_{k=1}^{N_f}\left(\frac{\partial\tilde{H}_{pe}(\nu_k;\theta)}{\partial\theta}\right)\frac{1}{\sigma^2_{|\hat{H}_{pe}|}(\nu_k)}\left(\frac{\partial\tilde{H}_{pe}(\nu_k;\theta)}{\partial\theta}\right)^*\right\}$$
$$+ \frac{2}{N_f}\,\mathrm{Re}\left\{\sum_{k=1}^{N_f}\left(\frac{\partial\tilde{H}_{px}(\nu_k;\theta)}{\partial\theta}\right)\frac{1}{\sigma^2_{|\hat{H}_{px}|}(\nu_k)}\left(\frac{\partial\tilde{H}_{px}(\nu_k;\theta)}{\partial\theta}\right)^*\right\} \tag{A4}$$

For a more in-depth derivation, the reader is referred to [34]. The CRLB does not always accurately reflect the true parameter variance [52]. This can be due to incorrect assumptions about noise in the measurement loop or due to modeling errors. Also the nonlinearity of an estimation problem appears to contribute significantly. This is why it only serves as an indication of the variance in the parameter vector and it is not compared with the variance found in the Monte Carlo simulations of Sec. V.

References

[1] McRuer, D. T., Graham, D., Krendel, E. S., and Reisener, W., "Human Pilot Dynamics in Compensatory Systems. Theory, Models and Experiments With Controlled Element and Forcing Function Variations," Wright–Patterson AFB, OH, Air Force Flight Dynamics Laboratory, AFFDL-TR-65-16, 1965.

[2] Krendel, E. S., and McRuer, D. T., "A Servomechanics Approach to Skill Development," *Journal of the Franklin Institute*, Vol. 269, No. 1, 1960, pp. 24–42. doi:10.1016/0016-0032(60)90245-3

[3] McRuer, D. T., and Jex, H. R., "A Review of Quasi-Linear Pilot Models," *IEEE Transactions on Human Factors in Electronics*, Vol. 8, No. 3, 1967, pp. 231–249.

[4] van Lunteren, A., and Stassen, H. G., "On the Variance of the Bicycle Rider's Behavior," *Proceedings of the Sixth Annual Conference on Manual Control*, Air Force Institute of Technology, Wright–Patterson AFB, OH, 7–9 April 1970, pp. 701–722.

[5] Vinje, E. W., and Pitkin, E. T., "Human Operator Dynamics for Aural Compensatory Tracking," *Seventh Annual Conference on Manual Control*, University of Southern California, Los Angeles, CA, 2–4 June 1971, pp. 339–348.

[6] van Lunteren, A., "Identification of Human Operator Describing Function Models with One or Two Inputs in Closed Loop Systems," Ph.D. Dissertation, Faculty of Aerospace Engineering, Delft University of Technology, Delft, The Netherlands, 1979.

[7] van Lunteren, A., and Stassen, H. G., "Parameter Estimation in Linear Models of the Human Operator in a Closed Loop with Application of Deterministic Test Signals," *Proceedings of the Ninth Annual Conference on Manual Control*, Massachusetts Institute of Technology, Cambridge, MA, 23–25 May 1973, pp. 289–298.

[8] Agarwal, G. C., Miura, H., and Gottlieb, G. L., "Computational Problems in Human Operator ARMA Models," *Eighteenth Annual Conference on Manual Control*, Air Force Institute of Technology, Wright–Patterson AFB, OH, 8–10 June 1982, pp. 58–74.

[9] Agarwal, G. C., Osafo-Charles, F., O'Neill, W. D., and Gottlieb, G. L., "Modeling of Human Operator Dynamics in Simple Manual Control Utilizing Time Series Analysis," *Proceedings of the Sixteenth Annual Conference on Manual Control*, Massachusetts Institute of Technology, Cambridge, MA, 5–7 May 1980, pp. 1–28.

[10] Altschul, R. E., Nagel, P. M., and Oliver, F., "Statistical Time Series Models of Pilot Control With Applications to Instrument Discrimination," *Proceedings of the Twentieth Annual Conference on Manual Control*, NASA Ames Research Center, Moffett Field, CA, June 12–14 1984, pp. 41–76.

[11] Bekey, G., and Hadaegh, F. Y., "Structure Errors in System Identification," *Proceedings of the Twentieth Annual Conference on Manual Control, NASA Ames Research Center*, 12–14 June 1984, pp. 149–156.

[12] Biezad, D., and Schmidt, D. K., "Time Series Modeling of Human Operator Dynamics in Manual Control Tasks," *Proceedings of the Twentieth Annual Conference on Manual Control*, NASA Ames Research Center, Moffett Field, CA, 12–14 June 1984, pp. 1–40.

[13] Holden, F. M., and Shinners, S. M., "Identification of Human Operator Performance Models Utilizing Time Series Analysis," *Proceedings of the Ninth Annual Conference on Manual Control*, Massachusetts Institute of Technology, Cambridge, MA, 23–25 May 1973, pp. 301–310.

[14] Jewell, W. F., "Application of a Pilot Control Strategy Identification Technique to a Joint FAA/NASA Ground-Based Simulation of Head-Up Displays for CTOL Aircraft," *Proceedings of the Sixteenth Annual Conference on Manual Control*, Massachusetts Institute of Technology, Cambridge, MA, 5–7 May 1980, pp. 395–409.

[15] Kugel, D. L., "Determination of In-Flight Pilot Parameters Using a Newton-Raphson Minimization Technique," *Proceedings of the Tenth Annual Conference on Manual Control*, Air Force Institute of Technology, Wright–Patterson AFB, OH, 9–11 April 1974, pp. 79–86.

[16] Merhav, S. J., and Gabay, E., "A Method for Unbiased Parameter Estimation by Means of the Equation Error Input Covariance," *Proceedings of the Tenth Annual Conference on Manual Control*, Air Force Institute of Technology, Wright–Patterson AFB, OH, 9–11 April 1974, pp. 39–60.

[17] Ninz, N. R., "Parametric Identification of Human Operator Models," *Proceedings of the Sixteenth Annual Conference on Manual Control*, Massachusetts Institute of Technology, Cambridge, MA, 5–7 May 1980, pp. 137–145.

[18] Schmidt, D. K., "Time Domain Identification of Pilot Dynamics and Control Strategy," *Eighteenth Annual Conference on Manual Control*, Air Force Institute of Technology, Wright–Patterson AFB, OH, 8–10 June 1982, pp. 19–40.

[19] Shirley, R. S., "A Comparison of Techniques for Measuring Human Operator Frequency Response," *Proceedings of the Sixth Annual Conference on Manual Control*, Air Force Institute of Technology, Wright–Patterson AFB, OH, 7–9 April 1970, pp. 803–870.

[20] Tanaka, K., Goto, N., and Washizu, K., "A Comparison of Techniques for Identifying Human Operator Dynamics Utilizing Time Series Analysis," *Proceedings of the Twelfth Annual Conference on Manual Control*, University of Illinois, Urbana, IL, 25–27 May 1976, pp. 673–693.

[21] Taylor, L. W., "A Look at Pilot Modeling Techniques at Low Frequencies," *Proceedings of the Sixth Annual Conference on Manual Control*, Air Force Institute of Technology, Wright–Patterson AFB, OH, 7–9 April 1970, pp. 871–896.

[22] Taylor, L. W., "A Comparison of Human Response Modeling in the Time and Frequency Domains," *Third Annual NASA-University Conference on Manual Control*, University of Southern California, Los Angeles, CA, 1–3 March 1967, pp. 137–156.

[23] Whitbeck, R. F., and Newell, F. D., "Mean Square Estimation of Human Pilot Transfer Functions," *Fourth Annual NASA-University Conference on Manual Control*, University of Michigan, Ann Arbor, MI, 21–23 March 1968, pp. 35–46.

[24] Stapleford, R. L., McRuer, D. T., and Magdaleno, R., "Pilot Describing Function Measurements in a Multiloop Task," *IEEE Transactions on Human Factors in Electronics*, Vol. 8, No. 2, 1967, pp. 113–125.

[25] Stapleford, R. L., Peters, R. A., and Alex, F. R., "Experiments and a Model for Pilot Dynamics with Visual and Motion Inputs," NASA CR-1325, 1969.

[26] Stapleford, R. L., Craig, S. J., and Tennant, J. A., "Measurement of Pilot Describing Functions in Single-Controller Multiloop Tasks," NASA, TR CR-1238, 1969.

[27] van Paassen, M. M., "Biophysics in Aircraft Control, A Model of the Neuromuscular System of the Pilot's Arm," Ph.D. Dissertation, Faculty of Aerospace Engineering, Delft University of Technology, Delft, The Netherlands, 1994.

[28] Teper, G. L., "An Effective Technique for Extracting Pilot Model Parameter Values from Multifeedback, Single-Input Tracking Tasks," *Proceedings of the Eighth Annual Conference on Manual Control*, University of Michigan, Ann Arbor, MI, 1972, pp. 23–33; also AFFDL Paper TR-72-92.

[29] Weir, D. H., and McRuer, D. T., "Pilot Dynamics for Instrument Approach Tasks: Full Panel Multiloop and Flight Director Operations," NASA, TR CR-2019, 1 May 1972.

[30] Weir, D. H., Heffley, R. K., and Ringland, R. F., "Simulation Investigation of Driver/Vehicle Performance in a Highway Gust Environment," *Proceedings of the Eighth Annual Conference on Manual Control*, University of Michigan, Ann Arbor, MI, 1972, pp. 449–465; also AFFDL Paper TR-72-92.

[31] Junker, A. M., Repperger, D. W., and Neff, J. A., "A Multiloop Approach to Modeling Motion Sensor Responses," *Proceedings of the Eleventh Annual Conference on Manual Control*, NASA Ames Research Center, Moffett Field, CA, 21–23 May 1975, pp. 645–655.

[32] Ringland, R. F., and Stapleford, R. L., "Motion Cue Effects on Pilot Tracking," *Seventh Annual Conference on Manual Control*, University of Southern California, Los Angeles, CA, 2–4 June 1971, pp. 327–338.

[33] van Paassen, M. M., and Mulder, M., "Identification of Human Operator Control Behaviour in Multiple-Loop Tracking Tasks," *Proceedings of the Seventh IFAC/IFIP/IFORS/IEA Symposium on Analysis, Design and Evaluation of Man-Machine Systems*, Pergamon, Kidlington, 16–18 Sept. 1998, pp. 515–520.

[34] Mulder, M., "Cybernetics of Tunnel-in-the-Sky Displays," Ph.D. Dissertation, Faculty of Aerospace Engineering, Delft University of Technology, Delft, The Netherlands, 1999.

[35] van Paassen, M. M., van der Vaart, J. C., and Mulder, J. A., "Model of the Neuromuscular Dynamics of the Human Pilot's Arm," *Journal of Aircraft*, Vol. 41, No. 6, Nov. 2004, pp. 1482–1490.

[36] Kaljouw, W. J., Mulder, M., and van Paassen, M. M., "Multi-Loop Identification of Pilot's Use of Central and Peripheral Visual Cues," AIAA Paper 2004-5443, 16–19 Aug. 2004.

[37] Löhner, C., Mulder, M., and van Paassen, M. M., "Multi-Loop Identification of Pilot Central Visual and Vestibular Motion Perception Processes," AIAA Paper 2005-6503, 15–18 Aug. 2005.

[38] Mulder, M., Kaljouw, W. J., and van Paassen, M. M., "Parameterized Multi-Loop Model of Pilot's Use of Central and Peripheral Visual Motion Cues," AIAA Paper 2005-5894, 15–18 Aug. 2005.

[39] Dehouck, T. L., Mulder, M., and van Paassen, M. M., "The Effects of Simulator Motion Filter Settings on Pilot Manual Control Behaviour," AIAA Paper 2006-6250, 21–24 Aug. 2006.

[40] Zaal, P. M. T., Nieuwenhuizen, F. M., Mulder, M., and van Paassen, M. M., "Perception of Visual and Motion Cues During Control of Self-Motion in Optic Flow Environments," AIAA Paper 2006-6627, 21–24 Aug. 2006.

[41] van der Vaart, J. C., "Modelling of Perception and Action in Compensatory Manual Control Tasks," Ph.D. Dissertation, Faculty of Aerospace Engineering, Delft University of Technology, Delft, The Netherlands, 1992.

[42] Hosman, R. J. A. W., "Pilot's Perception and Control of Aircraft Motions," Ph.D. Dissertation, Faculty of Aerospace Engineering, Delft University of Technology, Delft, The Netherlands, 1996.

[43] Hess, R. A., and Malsbury, T., "Closed-Loop Assessment of Flight Simulator Fidelity," *Journal of Guidance, Control, and Dynamics*, Vol. 14, No. 1, Jan.–Feb. 1991, pp. 191–197.

[44] Hess, R. A., Malsbury, T., and Atencio, A., Jr., "Flight Simulator Fidelity Assessment in a Rotorcraft Lateral Translation Maneuver," *Journal of Guidance, Control, and Dynamics*, Vol. 16, No. 1, Jan.–Feb. 1993, pp. 79–85.

[45] Zeyada, Y., and Hess, R. A., "Modeling Human Pilot Cue Utilization with Applications to Simulator Fidelity Assessment," *Journal of Aircraft*, Vol. 37, No. 4, July–Aug. 2000, pp. 588–597.

[46] Hess, R. A., and Siwakosit, W., "Assessment of Flight Simulator Fidelity in Multiaxis Tasks Including Visual Cue Quality," *Journal of Aircraft*, Vol. 38, No. 4, July–Aug. 2001, pp. 607–614.

[47] Zeyada, Y., and Hess, R. A., "Computer-Aided Asessment of Flight Simulator Fidelity," *Journal of Aircraft*, Vol. 40, No. 1, Jan.–Feb. 2003, pp. 173–180.

[48] Ljung, L., *System Identification Theory for the User*, 2nd ed., Prentice–Hall, Upper Saddle River, NJ, 1999.

[49] Fernandez, C., and Goldberg, J. M., "Physiology of Peripheral Neurons Innervating Semicircular Canals of the Squirrel Monkey. 2. Response to Sinusoidal Stimulation and Dynamics of Peripheral Vestibular System," *Journal of Neurophysiology*, Vol. 34, No. 4, 1971, pp. 661–675.

[50] Gordon-Smith, M., "An Investigation into Some Aspects of the Human Operator Describing Function While Controlling a Single Degree of Freedom," *Fifth Annual NASA—University Conference on Manual Control*, Massachusetts Institute of Technology, Cambridge, MA, 27–29 March 1969, pp. 203–240.

[51] Levison, W. H., and Kleinman, F. L., "A Model for Human Controller Remnant," *Fourth Annual NASA—University Conference on Manual Control*, University of Michigan, Ann Arbor, MI, 21–23 March 1968, pp. 3–14.

[52] Klein, V., "Estimation of Aircraft Aerodynamic Parameters from Flight Data," *Progress in Aerospace Sciences*, Vol. 26, No. 1, 1989, pp. 1–77. doi:10.1016/0376-0421(89)90002-X